ACS Sustainable Chemistry & Engineering

Research Article

pubs.acs.org/journal/ascecg

Controlling Pesticide Loss through Nanonetworks

Yubin Xiang,[†,§] Min Wang,[†,‡] Xiao Sun,[†,‡] Dongqing Cai,*[,†,‡] and Zhengyan Wu*[,†,‡]

[†]Key Laboratory of Ion Beam Bioengineering, Hefei Institutes of Physical Science, Chinese Academy of Sciences, Hefei 230031, People's Republic of China

[‡]Bioenergy Forest Research Center of State Forestry Administration, Hefei 230031, People's Republic of China

[§]School of Chemistry and Chemical Engineering, Anhui University, Hefei 230039, People's Republic of China

ABSTRACT: This work describes the feasibility of using high-energy electron beam (HEEB)-modified natural nanoclay (attapulgite) as an effective matrix to control the loss of pesticides that tend to discharge into the environment through washing and leaching, which causes severe pollution to both soil and groundwater. After irradiation by HEEB and because of thermal, charge, and impact effects, the originally aggregated attapulgite could be dispersed and form nanoporous networks, which could be beneficial for the binding of pesticides onto attapulgite. A loss control pesticide (LCP) was obtained when such attapulgite was added to a traditional pesticide. This pesticide–attapulgite complex could be retained by the rough surface of crop leaves, which increases the adhesion of pesticides on crop leaves and reduces pesticide loss, so that sufficient pesticides are supplied and the pollution risk of the pesticide is substantially lowered.

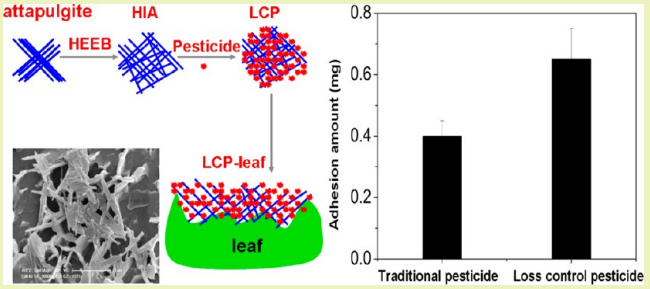

KEYWORDS: *High-energy electron beam, Attapulgite, Nanonetworks, Loss control, Pesticide*

INTRODUCTION

Pesticides are extensively applied in agriculture to combat weeds, pests, and diseases that are harmful to crop yields. Nevertheless, this has resulted in serious environmental pollution and ecological issues because as much as 90% of applied conventional pesticides do not work well because of degradation, volatilization, and leaching.[1,2] To compensate for migration and degradation losses and to ensure the effect remaining for an adequate period, pesticides are usually applied at concentrations greatly exceeding those required, increasing the likelihood of runoff and leaching and thus the risk of air and water contamination.[3]

Currently, the environmental problems associated with the use of highly mobile pesticides are becoming serious because the pesticide compounds are often detected in ground and surface waters.[4] Therefore, how to enhance the efficiency of pesticides and minimize their pollution has been an important topic in both agricultural and environmental chemistry, and many attempts in this subject have focused on regulating their loss behaviors. Controlled release formulations (CRF) are considered as a main pertinent alternative. The acting mechanism of CRF is to gradually release the active ingredients over time, thus limiting the amounts of ingredients immediately available for transport and degradation processes.[5−10] However, it is difficult to make the release period of pesticides exactly fit the pesticide-required periods of various crops. As a result, low utilization efficiency was sometimes obtained. In addition, the released pesticide compounds can still transfer to the environment and lead to severe pollution. Hence, we believe that controlling pesticide loss is a fundamental and promising countermeasure to reduce the environmental risk of pesticides. It is necessary to develop a new kind of pesticide with advantages of high adhesion capacity on plants, low loss amounts, long efficacy duration, and low dosage and cost, so as to decrease the risk of environmental pollution, save manpower by reducing the application frequencies, increase the safety of the pesticide user, and decrease the nontarget effects compared with traditional pesticides. Moreover, the prolonged efficacy duration of such a pesticide can be possible to meet the pesticide demand of crops during the growth period. In this article, we developed a loss control pesticide (LCP) through adding appropriate amount of attapulgite modified by a high-energy electron beam (HEEB).

Attapulgite ($(Mg,Al)_4(Si)_8(O,OH,H2O)_{26}\cdot nH_2O$), a kind of hydrated magnesium aluminum silicate, is an important mineral with fibrous morphology formed by nanorods with average dimensions of approximately 800−2000 nm in length and 30−40 nm in width.[11−14] The nanorod structure offers attapulgite a large specific surface area and high adsorption capacity and, thus, wide applications as filtration media, adsorbent, catalyst support, and so on.[15−17] Naturally, because of the high surface activity, attapulgite rods tend to aggregate with each other to form bunches, which is unfavorable for its application. Hence, it is important to improve the dispersion of attapulgite, which is

Received: December 10, 2013
Revised: January 14, 2014
Published: January 18, 2014

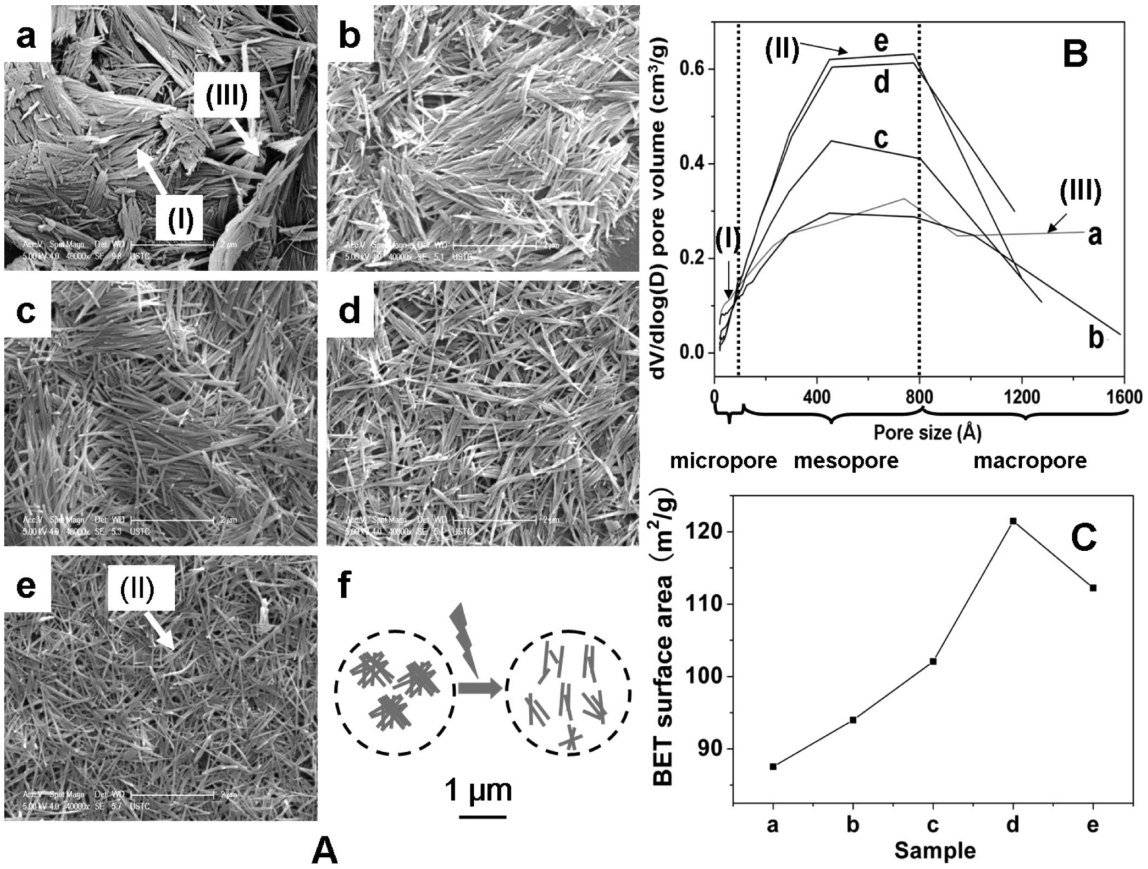

Figure 1. Morphology (A), PSD (B), and BSA (C) of NA (a), HIA10 (b), HIA20 (c), HIA30 (d), and HIA40 (e). (f) Schematic diagram of the improved dispersion of attapulgite treated with HEEB. (I) Micropores among the rods of a NA bunch. (II) Mesopores among single rods or small bunches of HIA40. (III) Macropores among NA bunches.

the dominant factor for its adsorption and carrier performance. Herein, natural attapulgite was modified using high-energy electron beam irradiation to separate the rods from each other to form a porous structure, and thus, more pesticide could be adsorbed onto attapulgite.

Because of the wide application for pest control in agriculture throughout the world, chlorpyrifos (CPF) (O,O-diethyl-O-(3,5,6-trichloro-2-pyridyl)-phosphorothioate), a broad spectrum organophosphorus insecticide, was selected as the model pesticide herein.[18−20] Chlorpyrifos can elicit a number of potential adverse impacts on the ecosystem or human health, including hepatic dysfunction, hematological, embryotoxicity, genotoxicity, teratogenicity, neurotoxicity, neurobehavioral changes, and so on.[21−24] Consequently, it is essential to control the transfer of CPF from crops to the soil and water. The objective of this study was to investigate the possibility of using attapulgite as an additive to increase the adhesion of CPF on crops and decrease the migration of CPF in soil so as to control the loss. Herein, we developed a novel loss control chlorpyrifos (LCC) using modified attapulgite treated with HEEB and investigated the adhesion and releasing performance of LCC on crop leaves and the migration performance in soil compared with natural attapulgite (NA). This work may provide a promising method to control pesticide loss and reduce the pollution risk to the environment.

MATERIALS AND METHODS

Materials. Natural attapulgite powder (100−200 mesh) was provided by Anbang Co., Ltd. (Anhui, China). Chlorpyrifos with a purity of 99% was provided by Jinghong Chemical Co. Ltd. (Jiangsu, China). Other chemicals, analytical reagent grade without any purification, were purchased from Sinopharm Chemical Reagent Company (Shanghai, China). Deionized water was used throughout this work.

HEEB Irradiation. Attapulgite samples in plastic bags (each 100 g) were irradiated by a high-energy electron beam accelerator (10 MeV and 10 kW) with fluences of 10, 20, 30, and 40 kGy at room temperature, and the resulting samples were designated as HIA10, HIA 20, HIA30, and HIA40, respectively.

LCC Emulsion Preparation. Chlorpyrifos (1.0 g) was dissolved in 20 mL of petroleum ether, and then 1 mL of Tween 80 was added to the solution. One milliliter of the the resulting solution was mixed with 40 mL of deionized water to obtain the CPF emulsion. Afterward, 0.1 g of HIA10, HIA20, HIA30, or HIA40 was added to 40 mL of chlorpyrifos emulsion to obtain the LCC emulsions.

Adhesion Performance Investigation. LCC emulsion (1 mL) was sprayed evenly onto a peanut leaf that lay on a Petri dish with a tilt angle of 30° on the ground at 30 °C. Then, in order to simulate the rainwater, 5 mL deionized water was sprayed evenly onto the resulting leaf. After air-drying, the leaf was immersed into 10 mL of petroleum ether and shaken for 10 min at 120 rpm to extract the remaining chlorpyrifos from the leaf surface to the petroleum ether solution. Finally, the concentration of chlorpyrifos in the petroleum ether solution was measured.

Releasing Performance Investigation. A part of a peanut leaf (2 cm × 2 cm) was placed into 20 mL of LCC (based on HIA40) or CPF emulsion and transferred into a Petri dish immediately. Then the CPF remaining amount (CRA) on the leaf surface with time was measured at room temperature to achieve the dynamic releasing performance of LCC and CPF. All the experiments were carried out in triplicate.

dx.doi.org/10.1021/sc400513p | ACS Sustainable Chem. Eng. 2014, 2, 918−924

Leaching Behavior Investigation. A total of 2.5 g of soil (150−200 mesh) was put into a 2.5 mL centrifuge tube, and a hole (diameter of 2 mm) was opened at the bottom. A little cotton was put below the soil layer to prevent the soil from leaching out. Three milliliters of LCC emulsion was added to the top of the soil layer dropwise. The leachate was collected and extracted with 6 mL of petroleum ether, and the concentration of chlorpyrifos in the petroleum ether was measured afterward.

Characterization. The morphology of attapulgite was observed on a scanning electron microscope (SEM) (Sirion 200, FEI Co., U.S.A.). The pore size distribution (PSD) and Braumer−Emmet−Teller surface area (BSA) of attapulgite were detected using a porosimetry analyzer (Tristar II, 3020M, Micromeritics Co., U.S.A.). The structure and interaction analyses were performed using a TTR-III X-ray diffractometer (XRD) (Rigaku Co., Japan) and a Fourier transform infrared spectrometer (FTIR) (Bruker Co., Germany). The concentration of chlorpyrifos in the petroleum ether was measured using a UV−vis spectrophotometer (UV 2550, Shimadzu Co., Japan) at a wavelength of 293 nm.

RESULTS AND DISCUSSION

Morphology and Microstructure Modification Investigation. Attapulgite mainly consists of silicon oxide, magnesium oxide, and aluminum hydrate and has poor thermal and electrical conductance. In our previous work,[25,26] it was found that NA bunches could disperse, bend, and cross-link with each other to form three-dimensional networks because of the thermal effect of ion beam bombardment (IBB). Therefore, the thermal effect of beam bombardment can play an important role in the dispersion of NA. When NA rods are bombarded by a high-energy and density electron beam, the thermal stress caused by the inhomogeneous distribution of heat along the NA axis can separate the rods from each other. Additionally, the poor electrical conductance of NA is beneficial for many electrons to accumulate on the surfaces of the rods when being irradiated by HEEB, so that the absolute values of the negative surface potentials of NA rods and eletrostatic repulsions among NA rods increase. Besides the thermal and charge effects, the physical impact effect caused by the high momentum of electrons can be another driving force for the dispersion of the aggregated NA.[27] Because of these three effects, the original big NA bunches (Figure 1A(a)) could be transformed to small ones after HEEB irradiation at fluences of 10 and 20 kGy (Figure 1A(b) and (c)). Furthermore, with the increase in fluence, the bunches of HIA30 became much smaller, and a number of single rods can be clearly seen (Figure 1A(d)). For HIA40, most of the small bunches dispersed further into single rods, and porous networks were formed by those single rods, as shown in Figure 1A(e). This morphology indicates that HEEB treatment can effectively enhance the dispersion of attapulgite (schematic diagram, Figure 1A(f)), and the dispersion degree increases with the fluence, wherein the main mechanism can probably be attributed to the thermal, charge, and impact effects of HEEB.

In order to further investigate this dispersion process, the PSD and BSA of NA- and HEEB-irradiated attapulgite (HIA) were analyzed. As shown in Figure 1B, the amount of the pore with a certain diameter (APCD) could be represented by dV/dlog(D) pore volume, where D is the pore diameter, and V is the total pore volume. The APCD (>120 nm) of HIA was lower than that of NA. The APCD (80−120 nm) of HIA decreased with the pore diameter, and the decrease rate grew with the fluence of the HEEB. For the pores (10−80 nm), the APCD of HIA increased with the fluence, wherein the APCD of HIA20 was obviously higher than that of HIA10, which is similar to that of NA. Furthermore, the APCDs of HIA30 and HIA40 increased significantly compared with HIA20. Nevertheless, the APCD (<10 nm) of the samples decreased with the increasing fluence. The PSD analysis indicates that with the increase in HEEB fluence, both macropore (>80 nm) and micropore (<10 nm) amounts decrease, while the amounts of mesopore (10−80 nm) increases. This is because HEEB treatment makes the amounts of big HIA bunches decrease and the amounts of small bunches increase. Thus, the amounts of macropores (arrow (III), Figure 1A) among these big bunches decrease, and the amounts of mesopores (arrow (II), Figure 1A) among small bunches or single rods increase. In addition, with the increase in HEEB fluence, more and more micropores (arrow (I), Figure 1A) among rods of the bunches enlarged and tranformed into mesopores, resulting in decreasing amounts of micropores. Hence, NA possesses the most macropores, especially those greater than 120 nm (arrow (III), Figure 1B), and micropores (arrow (I), Figure 1B), while HIA40 possesses the most mesopores (arrow (II), Figure 1B). Therefore, the PSD results of NA and HIA are consistent with those of morphology.

BSA, closely related to the adsorption capacity of attapulgite, was also investigated. Figure1C illustrates that the BSA of these attapulgite samples increases substantially with the HEEB fluence from 0 to 30 kGy and decreases thereafter (30−40 kGy). This result indicates that the BSA of attapulgite is determined by dispersion degree. For NA, the rods attach to each other so tightly that the rod surface is partially exposed, and thus, the BSA is rather small. After HEEB irradiation, those aggregated rods were separated from each other, and the mean distance among the rods increased with the electron fluence (0−30 kGy), resulting in larger exposed rod surface areas and thus higher BSA. However, the rods of HIA40 were so dispersed that the mean diameter of the formed mesopores (actually the mean distance among the rods) is rather high, and thus, the BSA of HIA40 is lower compared with HIA30. That is to say, the BSA results agree well with the morphology and PSA results.

X-ray diffraction measurements were performed to investigate the crystal structure information of attapulgite before and after HEEB treatment. As shown in the XRD spectra (Figure 2), no obvious new peaks or peak shifts were found in HIA20 and HIA40 compared with NA, indicating that no new substance is generated and no obvious chemical reaction

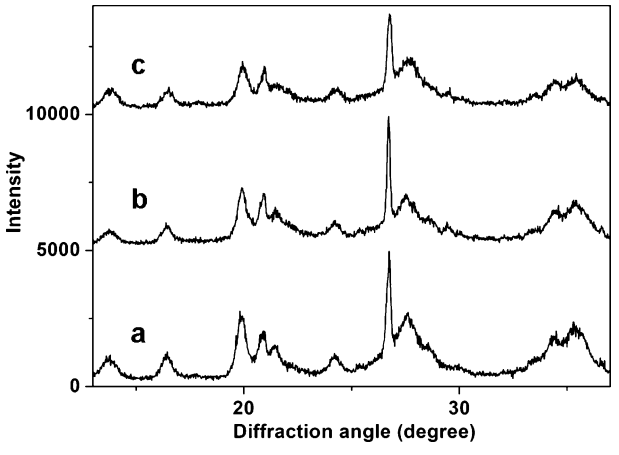

Figure 2. XRD spectra of NA (a), HIA20 (b), and HIA40 (c).

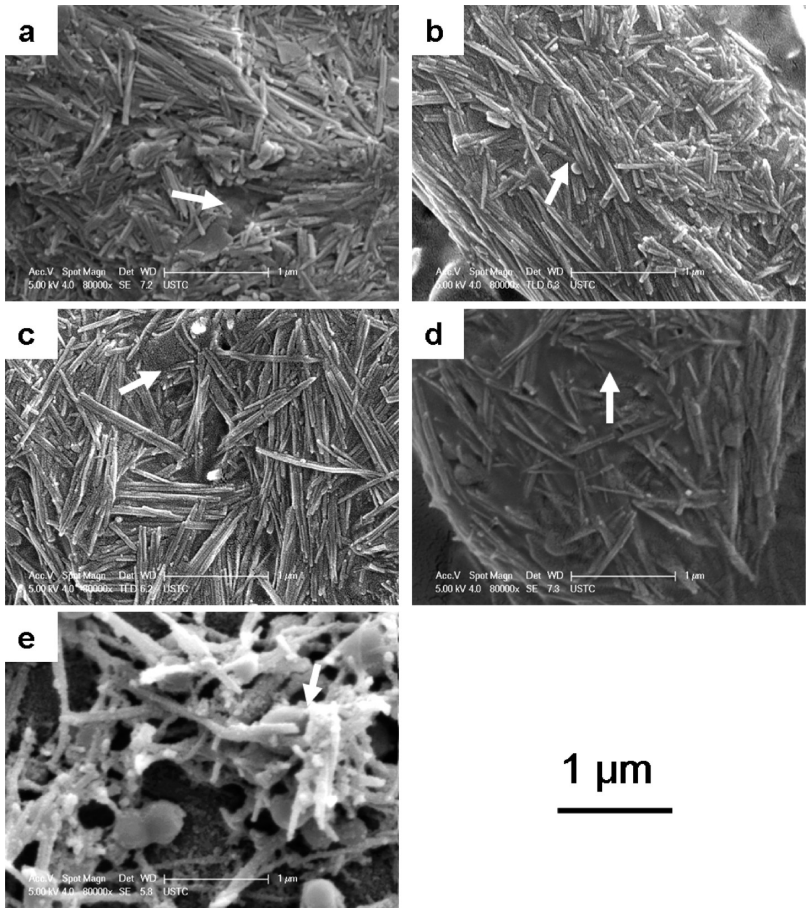

Figure 3. Morphology of LCC based on NA (a), HIA10 (b), HIA20 (c), HIA30 (d), and HIA40 (e).

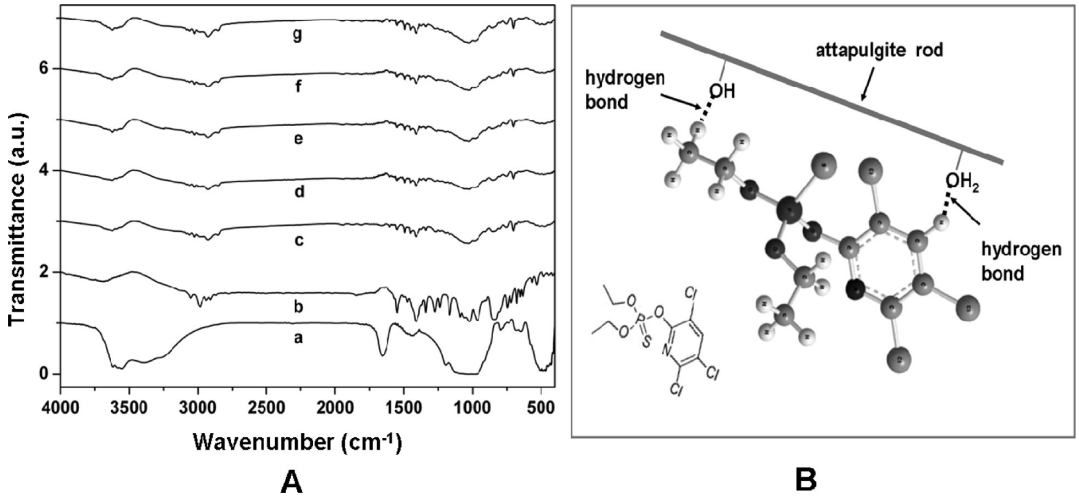

Figure 4. (A) FTIR spectra of NA (a), CPF (b), LCC based on NA (c), HIA10 (d), HIA20 (e), HIA30 (f), and HIA40 (g). (B) Schematic diagram of the hydrogen bonds between attapulgite and CPF.

occurred during the HEEB irradiation process. Nevertheless, after irradiation, most of the main characteristic peaks (19.8° (040), 27.38° (400), and 25.26° (102)) of attapulgite became more and more weakened with the increasing fluence (20−40 kGy), probably because of the decreasing order of degree of the rods resulting from the improved dispersion. This result is also in accordance with the preceding morphology and PSD and BSA results, and all of these prove the high availability of dispersing attapulgite using HEEB.

Interaction Analysis between HIA and CPF. To investigate the interaction between attapulgite and CPF, the morphologies of LCC prepared by the addition of NA or HIA were observed. As shown in Figure 3, much more CPF could occupy the pores (noted by the arrows in Figure 3) of HIA, which appeared more porous than NA. With the increase in HEEB fluence, the porosity of HIA and thus the amounts of adsorbed CPF increased significantly. Although HIA40 possesses smaller BSA compared with HIA30, HIA40 can

dx.doi.org/10.1021/sc400513p | ACS Sustainable Chem. Eng. 2014, 2, 918−924

hold more CPF. This is probably attributed to its 3D porous network structure (Figures 1A(e) and 3(e)). That is to say, quite a large amount of CPF is held in the pores among rods of HIA besides being adsorbed on the rod surface. In other words, the porosity (actually the dispersion degree) is the key factor dominating the adsorption and holding performance of attapulgite for CPF. Generally, nanomaterials with network structures could possess high porosity and adsorption capacity.[28−30] In conclusion, HEEB treatment can effectively enhance the adsorption and holding ability for CPF, which is mainly dependent on the dispersion of attapulgite.

To further analyze the interaction between attapulgite and CPF, FTIR spectra of LCC system were investigated, and the result is illustrated in Figure 4A. Peaks of both CPF (1542 cm^{-1} for C═N and 1412 cm^{-1} for pyridine stretching vibrations) and attapulgite (793 cm^{-1} for Si−O−Si and 3546 cm^{-1} for OH_2 stretching vibrations) are clearly shown in Figure 4A(c)−(g), indicating that CPF is successfully adsorbed onto NA and HIA. Moreover, the relative strength of the characteristic peaks (2917 cm^{-1} for C−H, 1542 cm^{-1} for C═N, and 1412 cm^{-1} for pyridine stretching vibrations) in Figure 4A(g) appeared higher compared with Figure 4A(c)−(f) because of the relatively higher amount of adsorbed CPF on HIA40. In addition, the CPF peaks (3039 cm^{-1} for −CH on the pyridine ring and 2978 cm^{-1} for $-CH_3$ in the branch chain) were red-shifted to 3018 and 2917 cm^{-1} in LCC (Figure 4A(c)-(g)), which is probably because of the formation of hydrogen bonds between CPF (−CH on the pyridine ring or $-CH_3$ in the branch chain) and attapulgite (−OH or OH_2) (Figure 4B). Some CPF molecules are adsorbed onto the rod surface through hydrogen bonds, and some molecules not near to the surface are probably held in the pores among rods through the intramolecular hydrogen bonds (actually the intermolecular association effect). From the FTIR analysis, a conclusion can be drawn that hydrogen bonds are probably the main interaction for the adsorption and holding performance of attapulgite on CPF molecules.

Besides, the XRD patterns of the LCC system were investigated to obtain the crystal structure changes of HIA in LCC compared with NA. As shown in Figure 5, no obvious new peak or peak shift is found in the spectra of LCC based on HIA20 or HIA40 compared with LCC based on NA, demonstrating that no obvious chemical reaction occurred between attapulgite and CPF, and almost no CPF molecules intercalated the crystal layer of attapulgite. In other words, CPF molecules are mainly adsorbed on the surfaces of the rods or held in the pores among rods through physical interaction or hydrogen bonds between attapulgite and CPF. That is why the dispersion and porosity of attapulgite is so important for the adsorption and holding performance on CPF.

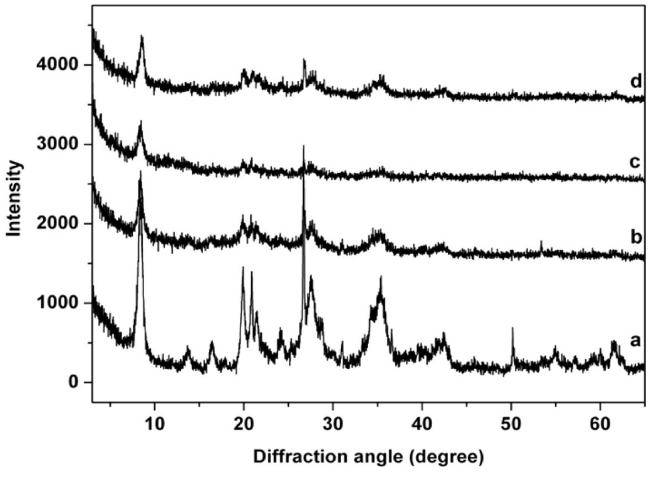

Figure 5. XRD spectra of NA (a), LCC based on NA (b), HIA20 (c), and HIA40 (d).

Adhesion Performance of LCC on Leaf Surface. Naturally, there are plenty of micro/nanoflakes on the peanut leaf surface, shown clearly in Figure 6B and C, resulting in a rough surface and thus a high retaining ability for attapulgite. This retaining ability increased with the decrease in the diameter of attapulgite particles because small attapulgite particles possess high surface activity and thus can attach tightly to the micro/nanoflakes on the peanut leaf surface. According to the preceding analysis, the dispersion of attapulgite was improved effectively with increasing HEEB fluence, which means more and more attapulgite bunches were dispersed. Therefore, the retaining ability of the rough surface for attapulgite could increase with the HEEB fluence, especially for HIA40, which possesses the nanonetwork structure fabricated by a great number of single attapulgite rods. Furthermore, based on the above investigations, the adsorption and holding performance of attapulgite for CPF also increased with the irradiation fluence. That is to say, both the retaining performance of the surface and the binding ability of attapulgite with CPF increase with the fluence, and thus the adhesion capacity of LCC increased significantly compared with CPF alone (Figure 6E(g)). Moreover, the antiwashing ability of LCC also increased with the fluence, resulting in a lower loss amount of CPF compared with CPF alone (Figure 6E(h)). The schematic diagram of the fabrication procedure of LCC (Figure 6A) and its adhesion state on the crop leaf (Figure 6D) were illustrated. This result indicates that HIA could effectively improve the adhesion performance of CPF on the peanut leaf surface, resulting in a high antiwashing capacity and low CPF loss amount, so that the utilization efficiency of CPF increased, which is mainly attributed to the high binding and retaining capacities of HIA. As a result, the migration and loss of pesticide from the crop leaf surfaces could be controlled, which is favorable for reducing the environmental risk of pesticides.

Releasing Performance of LCC on Leaf Surface. CPF on the leaf could be released from the network structure of LCC. A part of the released CPF could enter the atmosphere through volatilization, and the other part could be absorbed by the leaf. To obtain the release performance of LCC based on HIA40, the CRA on the leaf surface was determined every hour. As shown in Figure 7, LCC exhibited a higher initial CRA (actually the adhesion amount) compared with CPF, which was consistent with the preceding adhesion performance analysis. The CRAs of both LCC and CPF decreased with time, wherein LCC decreased more slowly than CPF. Moreover, CRA of LCC nearly reached equilibrium at the fourth hour, while CRA of CPF still decreased obviously within six hours. This result demonstrated that LCC could effectively control the release behavior of CPF resulting in a high remaining amount on the leaf surface, which was favorable for the prolongation of the efficacy duration.

Leaching Performance of LCC inSoil. HIA can not only increase the adhesion capacity of CPF on the leaf surface but can also reduce the leaching loss through the soil. As shown in Figure 8B, the leaching loss ratio of LCC decreased with the increasing HEEB fluence compared with CPF alone, which is because of the gradual increase in the binding ability of HIA for

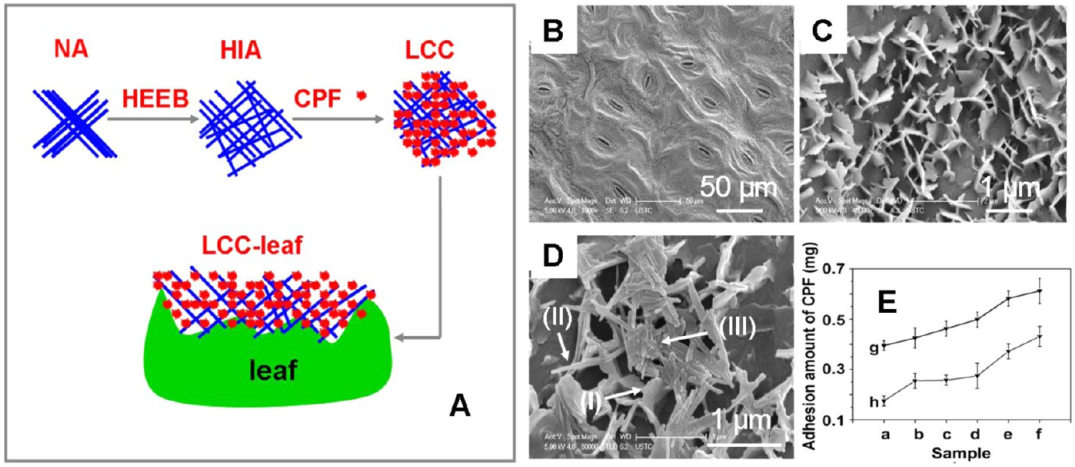

Figure 6. (A) Schematic diagram of the fabrication procedure of LCC and its adhesion state on crop leaves. (B) Morphology of the leaf surface of peanut. (C) Magnified image of (B). (D) LCC retained on the rough peanut leaf surface, wherein (I)−(III) represent a wrinkled flake of peanut leaf, an attapulgite rod, and CPF, respectively. (E) Adhesion performance of CPF (a) and LCC based on NA (b), HIA10 (c), HIA20 (d), HIA30 (e), and HIA40 (f) on a leaf surface before (g) and after (h) washing with simulated rainwater.

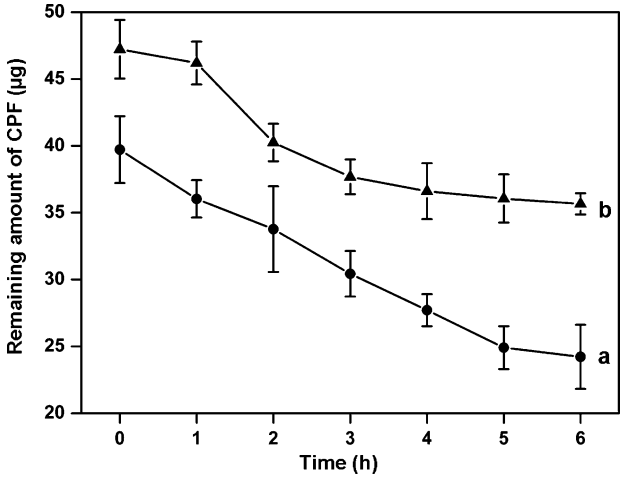

Figure 7. Releasing performance of CPF (a) and LCC based on HIA40 (b) on the peanut leaf surface.

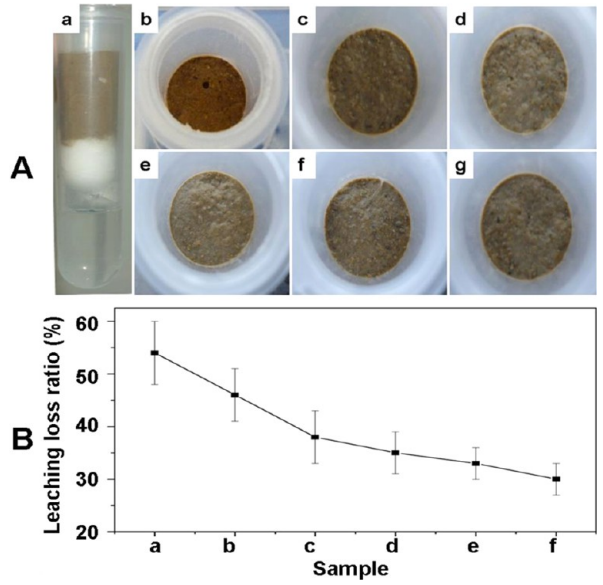

Figure 8. (A) Images of the soil column (a) and the soil surface after leaching of CPF (b) and LCC based on NA (c), HIA10 (d), HIA20 (e), HIA30 (f), and HIA40 (g). (B) Leaching loss ratios of CPF (a) and LCC based on NA (b), HIA10 (c), HIA20 (d), HIA30 (e), and HIA40 (f).

CPF. LCC tended to be retained on the soil surface, making the soil surface much whiter than that of the CPF alone (Figure 8A). Thus, the leaching loss of CPF was reduced, and more CPF could be kept in the top soil layer, which is a benefit to the photolysis and biolysis of CPF thereafter. In addition, this control of pesticide migration in soil could also help to protect groundwater.

CONCLUSIONS

In this article, an approach for controlling CPF loss was described using LCC obtained by adding HIA to CPF. The results demonstrate that HEEB treatment could effectively improve the dispersion of attapulgite because of thermal, charge, and impact effects. As a result, a highly porous network structure was obtained, and CPF could be adsorbed and held in the network. On basis of the high binding and retaining performance of HIA, LCC showed a higher adhesion capacity and a slower releasing performance on the crop leaf surface and a lower leaching loss ratio in the soil compared with CPF alone, which may help to improve the utilization efficiency of CPF and decrease the environmental risk.

AUTHOR INFORMATION

Corresponding Authors

* Tel.: +86-551-65595012. Fax: +86-551-65591413. E-mail: dqcai@ipp.ac.cn (D.C.).
* Tel.: +86-551-65595012. Fax: +86-551-65591413. E-mail: zywu@ipp.ac.cn (Z.W.).

Notes

The authors declare no competing financial interest.

ACKNOWLEDGMENTS

The authors acknowledge financial support from the Key Program of Chinese Academy of Sciences (No. KSZD-EW-Z-022-05) and the Scientific and Technological Project of Anhui Province (No. 1206c0805014).

REFERENCES

(1) Ravier, I.; Haouisee, E.; Clément, M.; Seux, R.; Briand, O. Field experiments for the evaluation of pesticide spray-drift on arable crops. *Pest Manage. Sci.* **2005**, *61*, 728−736.

(2) Mogul, M. G.; Akin, H.; Hasirci, N.; Trantolo, D. J.; Gresser, J. D.; Wise, D. L. Controlled release of biologically active agents for purposes of agricultural crop management. *Resour., Conserv. Recycl.* **1996**, *16*, 289−320.

(3) Gerstl, Z.; Nasser, A.; Mingelgrin, U. Controlled release of pesticides into soils from clay-polymer formulations. *J. Agric. Food Chem.* **1998**, *46*, 3797−3802.

(4) Arias-Estévez, M.; López-Periago, E.; Martínez-Carballo, E.; Simal-Gándara, J.; Mejuto, J. C.; García-Río, L. The mobility and degradation of pesticides in soils and the pollution of groundwater resources. *Agric. Ecosyst. Environ.* **2008**, *123*, 247−260.

(5) Bahadir, M. Safe formulations of agrochemicals. *Chemosphere* **1987**, *16*, 615−621.

(6) Gerstl, Z.; Nasser, A.; Mingelgrin, U. Controlled release of pesticides into water from clay-polymer formulations. *J. Agric. Food Chem.* **1998**, *46*, 3803−3809.

(7) Celis, R.; Hermosin, M. C.; Carrizosa, M. J.; Cornejo, J. Inorganic and organic clays ascarriers for controlled release of the herbicide hexazinone. *J. Agric. Food Chem.* **2002**, *50*, 2324−2330.

(8) Bruna, F.; Pavlovic, I.; Celis, R.; Barriga, C.; Cornejo, J.; Ulibarri, M. A. Organohydrotalcites as novel supports for the slow release of the herbicide terbuthylazine. *Appl. Clay Sci.* **2008**, *42*, 194−200.

(9) Fernández-Pérez, M.; Villafranca-Sánchez, M.; González-Pradas, E.; Flores- Céspedes, F. Controlled release of diuron from an alginate-bentonite formulation: Water release kinetics and soil mobility study. *J. Agric. Food Chem.* **1999**, *47*, 791−798.

(10) Dailey, O. D. Volatilization of alachlor from polymeric formulations. *J. Agric. Food Chem.* **2004**, *52*, 6742−6746.

(11) Giustetto, R.; Xamena, F. X. L.; Ricchiardi, G.; Bordiga, S.; Damin, A.; Gobetto, R.; Chierotti, M. R. Maya Blue: A computational and spectroscope study. *J. Phys. Chem. B.* **2005**, *109*, 19360−19368.

(12) Huang, J.; Liu, Y.; Jin, Q.; Wang, X.; Yang, J. Adsorption studies of a water soluble dye, Reactive Red MF-3B, using sonication surfactant-modified attapulgite clay. *J. Hazard. Mater.* **2007**, *143*, 541−548.

(13) Chen, H.; Wang, A. Q. Kinetic and isothermal studies of lead ion adsorption onto palygorskite clay. *J. Colloid Interface Sci.* **2007**, *307*, 309−316.

(14) Xue, S. Q.; Reinholdt, M.; Pinnavaia, T. J. Palygorskite as an epoxy polymer reinforcement agent. *Polymer* **2006**, *47*, 3344−3350.

(15) Chisholm, J. E. An X-ray powder-diffraction study of palygorskite. *Can. Mineral.* **1990**, *28*, 329−339.

(16) Chiari, G.; Giustetto, R.; Ricchiardi, G. Crystal structure refinement of palygorskite and Maya Blue from molecular modeling and powder synchrotron diffraction. *Eur. J. Mineral.* **2003**, *15*, 21−33.

(17) Chisholm, J. E. Powder-diffraction patterns and structural models for palygorskite. *Can. Mineral.* **1992**, *30*, 61−73.

(18) Çetin, N.; Çetin, E.; Eraslan, G.; Bilgili, A. Chlorpyrifos induces cardiac dysfunction in rabbits. *Res. Vet. Sci.* **2007**, *82*, 405−408.

(19) Ambali, S. F.; Abbas, S. O.; Shittu, M.; Dzenda, T.; Kawu, M. U.; Salami, S. O.; Ayo, J. O. Effects of gestational exposure to chlorpyrifos on implantation and neonatal mice. *J. Cell Anim. Biol.* **2009**, *3*, 50−57.

(20) Saulsbury, M. D.; Heyliger, S. O.; Wang, K.; Johnson, D. J. Chlopyrifos induces oxidative stress in oligodendrocyte progenitor cells. *Toxicology* **2009**, *259*, 1−9.

(21) Ali, D.; Nagpure, N.; Kumar, S.; Kumar, R.; Kushwaha, B.; Lakra, W. Assessment of genotoxic and mutagenic effects of chlorpyrifos in freshwater fish *Channa punctatus* (Bloch) using micronucleus assay and alkaline single-cell gel electrophoresis. *Food Chem. Toxicol.* **2009**, *47*, 650−656.

(22) Qiao, D.; Seidler, F. J.; Slotkin, T. A. Oxidative mechanisms contributing to the developmental neurotoxicity of nicotine and chlorpyrifos. *Toxicol. Appl. Pharmacol.* **2005**, *206*, 17−26.

(23) Verma, R. S.; Mehta, A.; Srivastava, N. In vivo chlorpyrifos oxidative stress: Attenuation by antioxidant vitamins. *Pestic. Biochem. Phys.* **2007**, *88*, 191−196.

(24) Mehta, A.; Verma, R. S.; Srivastava, N. Chlorpyrifos induced alterations in the levels of hydrogen peroxide, nitrate and nitrite in rat brain and liver. *Pestic. Biochem. Phys.* **2009**, *94*, 55−59.

(25) Cai, D. Q.; Wu, Z. Y.; Jiang, J.; Ding, K. J.; Tong, L. P.; Chu, P. K.; Yu, Z. L. A unique technology of transforming inorganic nano-rods to nano-networks. *Nanotechnology* **2009**, *20*, 255302.

(26) Cai, D. Q.; Zhang, H.; Tang, Y.; Chu, P. K.; Yu, Z. L.; Wu, Z. Y. Nano-networks have better adsorption capability than nanorods. *Nano Commun. Networks.* **2010**, *1*, 257−263.

(27) Xiang, Y. B.; Wang, N.; Song, J. M.; Cai, D. Q.; Wu, Z. Y. Micro-nano pores fabricated by high energy electron beam irradiation: Suitable structure for controlling pesticide loss. *J. Agric. Food Chem.* **2013**, *61*, 5215−5219.

(28) Yang, J.; Zhou, Y. L.; Zheng, S. L.; Liu, X. F.; Qiu, X. H.; Tang, Z. Y.; Song, R.; He, Y. J.; Ahn, C. W.; Kim, J. W. Self-reorganization of CdTe nanoparticles into near-infrared $Hg_{1-x}Cd_xTe$ nanowire networks. *Chem. Mater.* **2009**, *21*, 3177−3182.

(29) Zheng, Z. Z.; Zhou, Y. L.; Li, X. Y.; Liu, S. Q.; Tang, Z. Y. Highly-sensitive organophosphorous pesticide biosensors based on nanostructured films of acetylcholinesterase and CdTe quantum dots. *Biosens. Bioelectron.* **2011**, *26*, 3081−3085.

(30) Yin, H. J.; Zhao, S. L.; Wan, J. W.; Tang, H. J.; Chang, L.; He, L. C.; Zhao, H. J.; Gao, Y.; Tang, Z. Y. Three-dimensional graphene/metal oxide nanoparticle hybrids for high-performance capacitive deionization of saline water. *Adv. Mater.* **2013**, *25*, 6270−6276.